Supporting Information:

Revealing Strain Induced Effects in Ultrathin Heterostructures at the Nanoscale

Syed Ghazi Sarwat, Martin Tweedie, Benjamin F Porter, Yingqiu Zhou, Yuewen Sheng, Jan Mol, Jamie Warner, Harish Bhaskaran*

Department of Materials, University of Oxford, Oxford, UL OX1 3PH

S1. Chemical Vapour Deposition Synthesis of Graphene and WS_2

WS2:

WS_2 was synthesized using S (300 mg) and WO_3 (200 mg) precurrsors (≥99.5%, Sigma-Aldrich) on a 2 by 2 cm silicon chip (300 nm SiO2) with a two furnaces system. Before insertion into the CVD quartz tube, the chip was thoroughly cleaned through sonication in acetone (15 min), in 2-propanal (15 min), followed by O_2 plasma clenaing (5 min). The tube with precursors and substrate inside was then put into the two furnaces, with S in first furnace and WO_3 in second. The system was flushed with 500 sccm Ar for at least 30 min (inorder to remove air), following which the first and second furnaces were set to ramp to 180 ℃ and 1170 ℃. The reaction process then lasted for 3 min (at Ar flow at 250 sccm and with the two furnaces stable at their set temperatures). After 3 min, the reaction was force stopped by decreasing Ar flow to 10 sccm, meanwhile, the first furnace was heated to 450 ℃ inorder to evaporate remaining S, and the second furance was cooled to room temperature. When the temperature of second furnace reached 950 ℃, Ar flow rate was ramped up of 500 sccm in order to blow away the S. Once the second furnace reached room temperature, the silicon chip was taken out of the chamber and processed for characterization

Graphene :

Large area uniform graphene was synthesized in a single furnace system on a polished copper foil. Methane was introduced as the gaseous carbon source for graphene nucleation and growth. The copper foil besides serving as the substrate also served as the catalyst. The whole system was first flushed with argon (1000 sccm), hydrogen (500 sccm) and methane (50 sccm) for 30 mins inorder to get rid-off any air in the quartz tube. The flow was then modulated (methane flow completely stopped, while Ar at 600 sccm and H2 at 300 sccm) and the temperature was ramped-up at 50℃/min to 1060 ℃ (see Ref[1] for temperature profiles) inorder to anneal Copper. Graphene growth was then carried-out at 1060 ℃ by introducing 20 sccm of methane (see Ref.[1] for flow rates) into the tube; the growth lasted for 1 Hr, after which the furnace was moved away and sample allowed to cool to room temperature

S2. Device Fabrication

A 2 by 2 cm PEN substrate was diced from a continuous 200 um thick PEN role using laser cutting. The two dimensional materials were transferred onto the PEN substrate using a non-aqueous sliding transfer method. Briefly, a Poly(methyl methacrylate) (PMMA) film was spun coated on the copper substarte containing graphene film. The copper foil was then placed on a $(NH_4)_2S_2O_8$ (0.1 M) solution inorder to etch away the copper. The remaining intact PMMA/graphene film was then transferred onto deionized water three times (in three different beakers) to get rid-off residual $(NH_4)_2S_2O_8$. A clean cover slide was dipped into the third beaker and graphene/PMMA film was scopped out from the beaker (it was ensured that the cover slide did not dry until the next step). The cover slide was placed at a 45^0 angle with respect to the PEN substrate and using a pipette, IPA was dropped on the cover slide. The IPA pushes the stack from the cover slide onto the PEN substrate. The IPA was then let to dry (first at room temperature, and then on a hotplate at 100℃ for 3 hours), leaving behind a uniformly oriented graphene film on PEN. For WS_2, the Si containing WS2 domains was first spin-coated with PMMA, following which the PMMA/WS_2 film was placed on a KOH solution (0.1 M) inorder to etch away SiO_2. Once etched, the floating PMMA/WS_2 film was scooped-out using a cover slide in a similar fashion as described eariler, and transferred using IPA droplets from a pipette onto the graphene covered PEN substrate. The substare was then annealed at 100℃ for 40 minutes.

S3. Optical Characterization

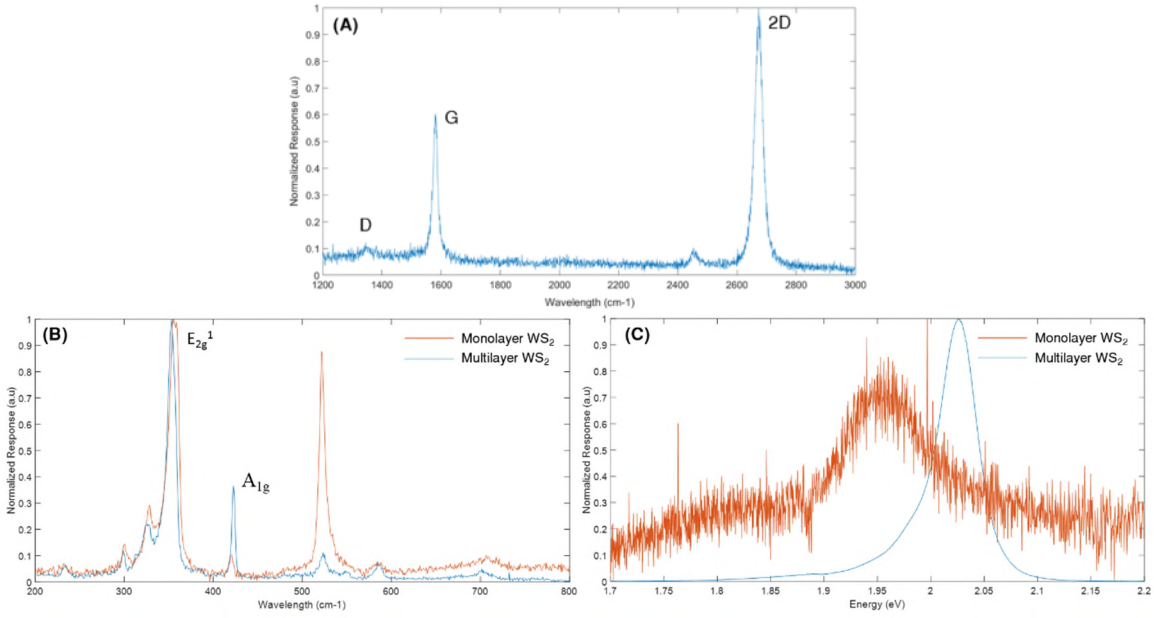

Figure S1. Optical Characterization on a Silicon Substrate (532 nm excitation). (A) Raman spectra of a transferred graphene on Silicon substrate. The singature peaks of graphene 2D and G are clearly evident, with their ratio

signifying graphene to be mono-layered. We however do observe scattered domains of bi-and trilayered graphene on this uniform mono-layered film. The D peak is indicative of defect/disorder in the lattice. (B) Normalized Raman spectra of mono and multi layered WS_2 after trasnfer on a silicon chip. The signature peaks of WS_2: E_{2g}^1 (354.64 cm-1) and A_{1g} (422.6 cm-1) are cleary evident. The E_{2g}^1 of multi-layered WS_2 is slightly red shifted (by 2 cm^{-1}) from that of monolayer WS_2, in agreement with the literature, while the A_{1g} perfectly coincide. The multi-layer WS_2 gives a much enhanced signal as opposed to monolayer counterpart owing to more number of layers, and (C) Normalized photoluminescence spectra (PL) of mono and multi layered WS_2 from the same spot as for the Raman suggesting good quality materials. PL signals of multi-layered WS_2 are severly suppressed due to its indirect band-gap as opposed to the monolayer WS_2 which has a direct band-gap (2 eV). Note the red-shift in multi-layered WS_2 which is likely from induced tensile strain during transfer (we note however that for transfer on PEN, no peak shift is observed)

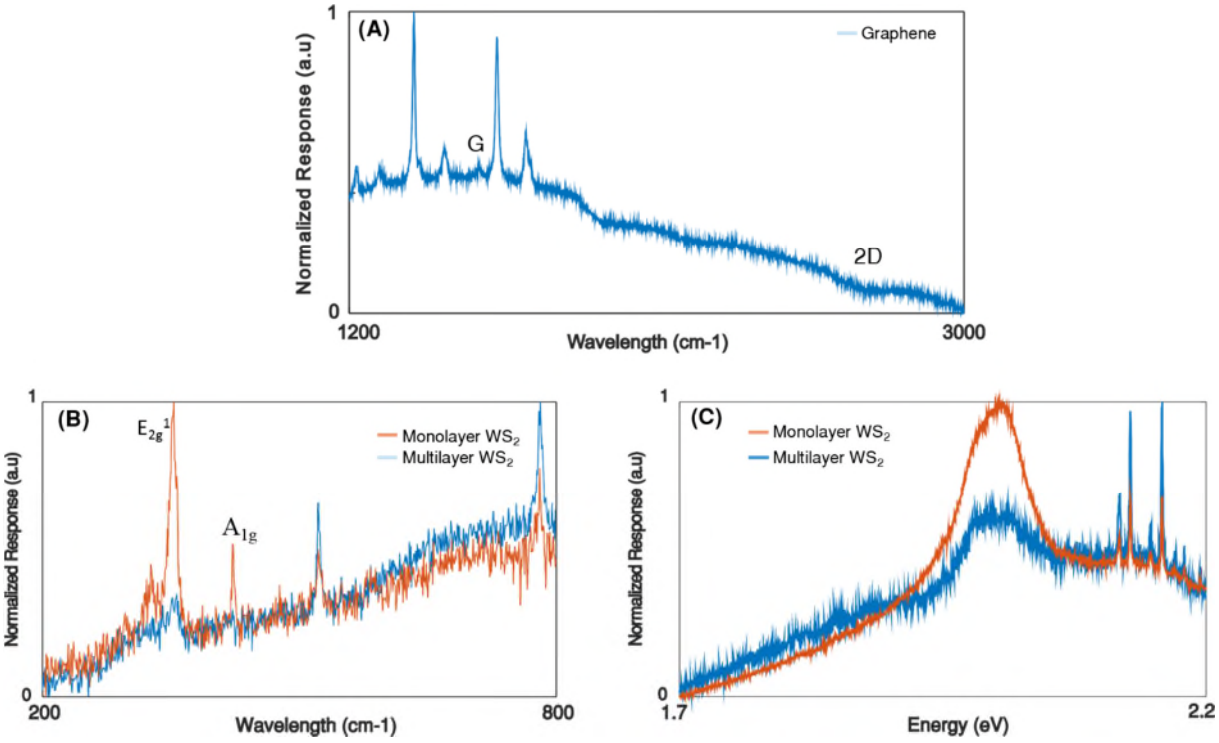

Figure S2. Optical Characterization on a PEN Subtrate (532 nm excitation). (A) Raman spectra of a transferred graphene on a PEN substarte. The singature peaks of graphene 2D and G are not evident, which is likely due to: overlapping (G) peaks and the suppression from hybridization and larger back ground noise (signal). (B) Normalized Raman spectra of mono and multi layered WS_2 after transfer on PEN. The signature peaks of monolayer WS_2: E_{2g}^1 (353 cm-1) and A_{1g} (420 cm-1) are cleary evident, with multi-layer producing an enhanced signal owing more number of layers, and (C) Normalized photoluminescence spectra (PL) of mono and multi layered WS_2 from the same spot as for the Raman. PL signals of multi-layered WS_2 are severly suppressed due to the indirect band-gap as opposed to monolayer WS_2 which has a direct band-gap (2.0 eV).

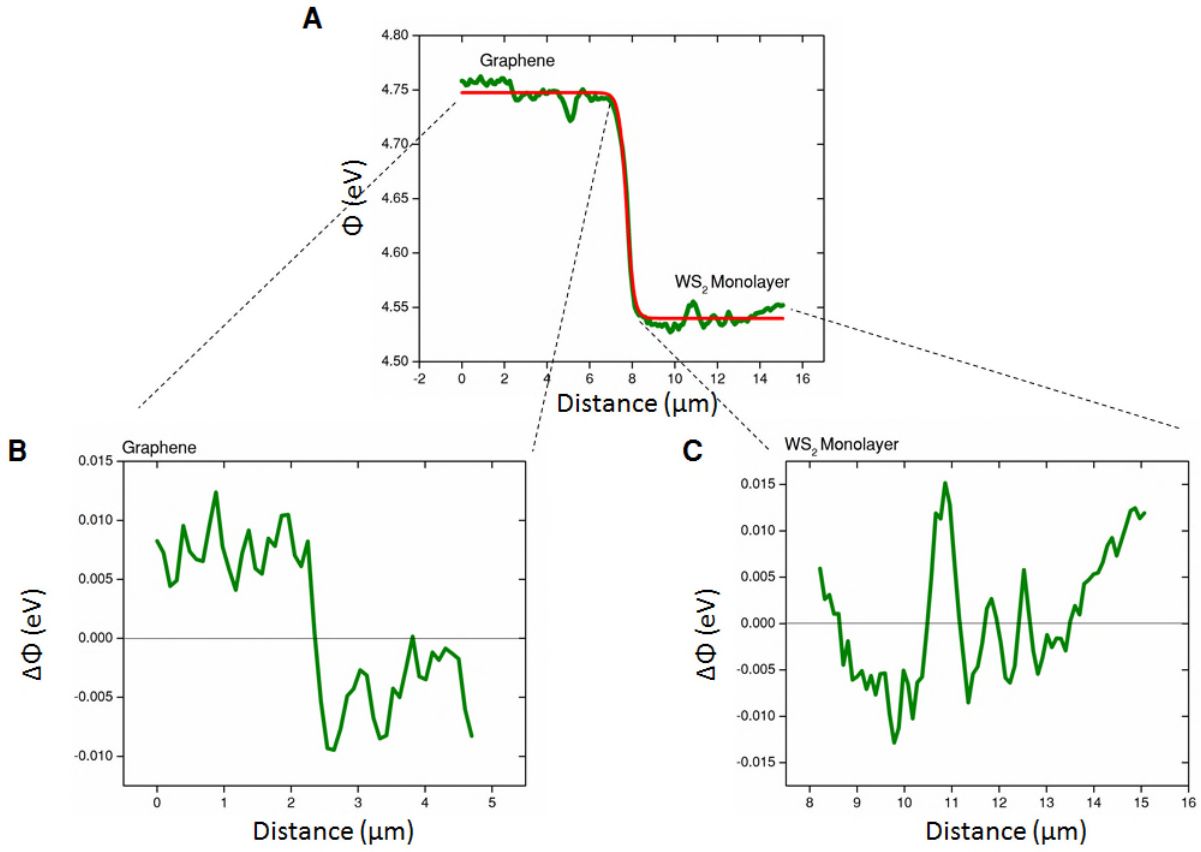

Figure S3. Work Function Extraction. (A) First the work function from the raw data (CPD) is computed using the equation $\Phi_{sample}(x,y) = \Phi_{tip} - e$ x $CPD(x,y)$, where Φ is the work function and then the work function trace (green trace) scan is fitted using a sigmoidal function (red trace). Best fitting parameters for the Y- Axis are as used as the work functions of the two dimensional materials. (B and C) Residual plots illustaing the error bars. Here the work function derived from the fitting is substracted from the the meaured work function at each point on the trace.

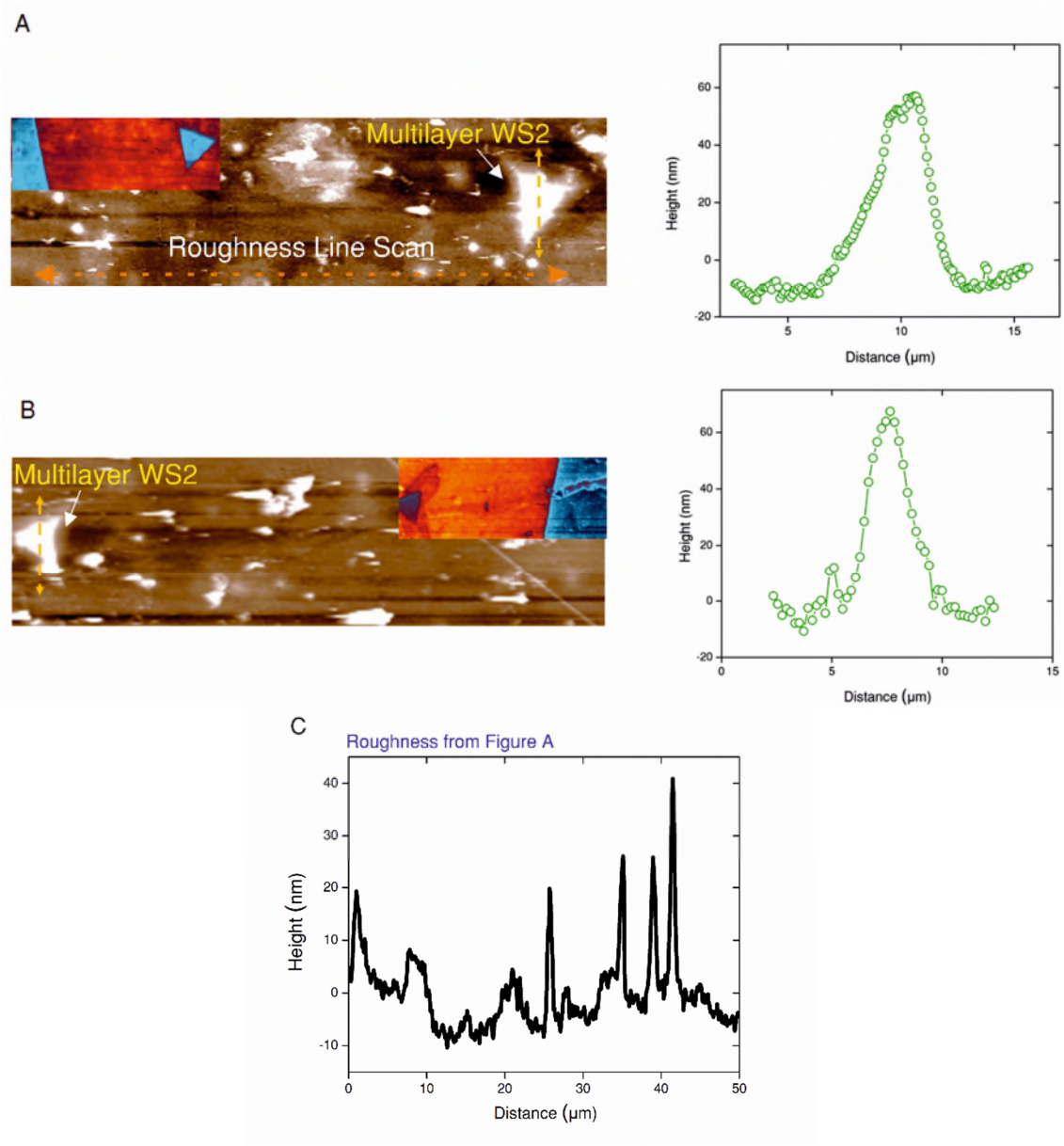

Figure S4 (A and B). Atomic force micrographs (sample 1 (A) and sample 2 (B)) of the Graphene/WS_2 heterostructure on PEN substrate. Monolayer WS_2 is indiscernible due its atomic thickness and high substrate roughness. Multi-layer WS_2 is discernible, and line scans across it are shown in the graphs. Thickness of multi-layer WS_2 in sample 1 and 2 is 64.4 nm and 72.2 nm (these numbers are likely to be not perfectly accurate due to substrate‘s high roughness), respectively, which are significantly large (81 layers for sample 1 and 91 layers for sample 2 to approximate multi-layered WS_2 in the bulk regime. Insets are the Kelvin Probe Micrographs, and (C) Line scan indicative of the substrate roughness. The root mean square value of roughness is 6.2 nm which is significantly higher than the thickness of monolayered Graphene (0.35-0.70 nm) and WS_2 (0.80 nm)

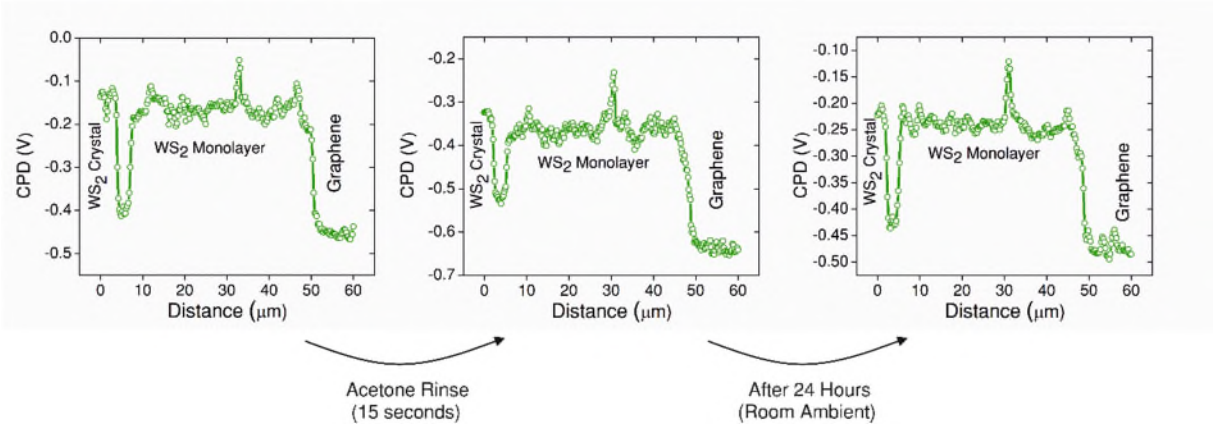

Figure S5 (A and B). (A) Influence of acetone on the two dimensional materials. Kelvin probe line spectra from sample 1 before, after and much after rinsing with acetone. Exposure to acetone results to an increase in the work function of WS_2 and Graphene indicative of *p*-doping, likely a result of the electron withdrawing nature of ester. The device almost recovers after 24 hours in room ambient. Note that Graphene and WS_2 react differently to acetone, resulting in changes in the junctions. Such a behaviour can be used in sensing applications (gas, temperature and solvents), and is a current subject of our focus. Similar variations in the work functions in response to variations in environment (humidity) have been demonstrated using KPM in both CVD and exfoliated forms of MoS_2[2,3] and graphene[4] suggesting this to be a tunebale intrinsic property of two dimensional materials, which arise from doping

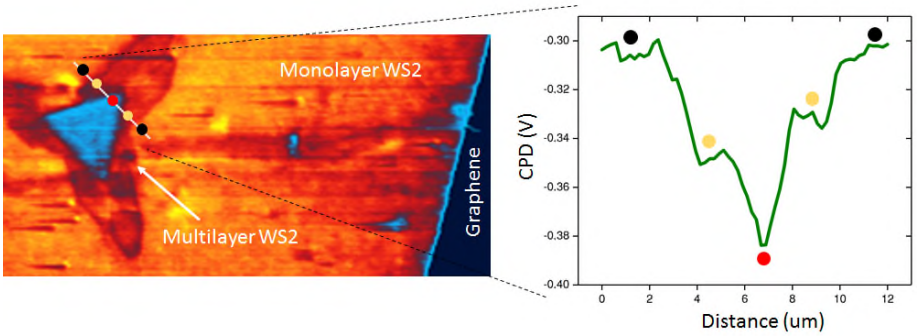

Figure S6. Thickness Dependency of Electrostatic Potential. Kelvin probe micrograph of a monolayer WS_2 domain with a flower shaped multilayer WS_2 domain in the centre. Such a structure evolves during CVD growth: first the triangular heterostructure nucleates, on boundries of which a monolayer WS_2 grows. The graph illsutrates the variation of contact potential difference, hence work funciton (increase) as a function of number of layers stacking monolayer WS_2

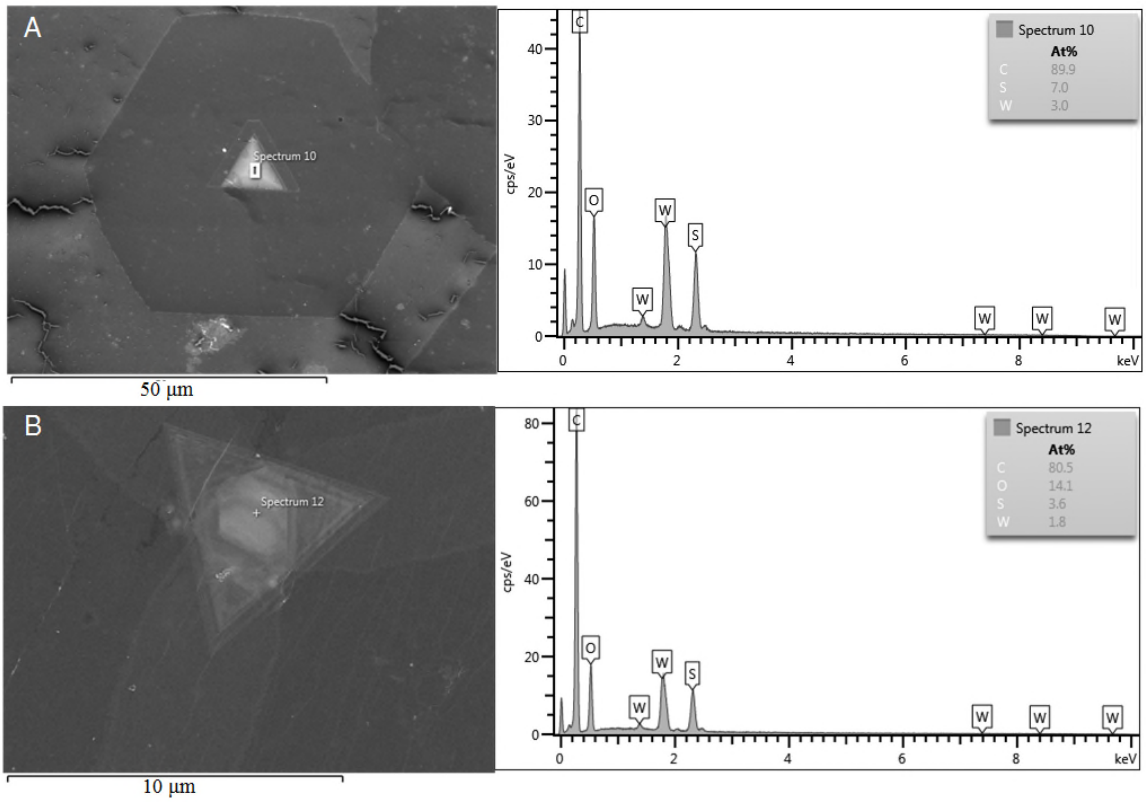

Figure S7 (A and B). Scanning electron micrographs of WS_2 domains on Graphene from sample 1(A) and sample 2(B) and corresponding energy dispersive X-ray point spectra. The differences observed in the work functions of multi-layer WS_2 in KPM is likely a result of the differences in the W:S ratio and the thickness (Figure S2). We also observe contamination in the form of residues (Figure A). We find that the most significant cause for contamination is from PMMA residues and dirt on the cover slides that is used for transfer. Transfer of graphene does not result in significant contaminants, while subsequent transfer of WS2 does. This is likely a result of strong WS_2-PMMA interaction.

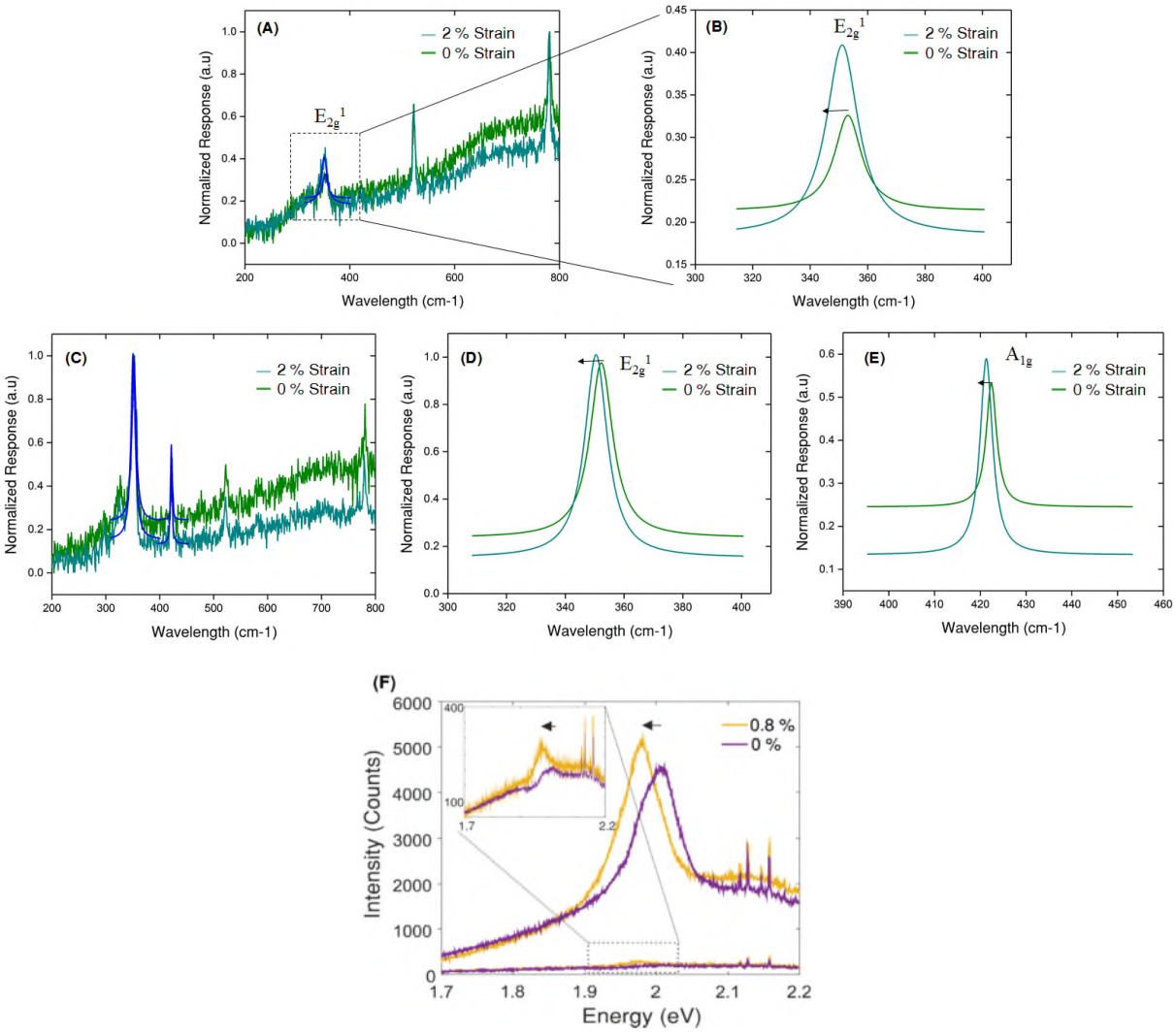

Figure S8. Optical Characterisation of Strain Effects (532 nm excitation) in WS_2. (A) Normalized Raman spectra of mono-layered WS_2 under 0 and 2 % strain. (B) The E_{2g}^1 (353.03 cm^{-1}) peak (fitted with Lorentzian function) red shifts by 2.2 cm^{-1} upon strain, indicative of lattice expansion, and is in agreement with literature. (C) Normalized Raman spectra of multi-layered WS_2 under zero and 2 % strain. (D) The E_{2g}^1 (352.11 cm^{-1}) peak (fitted with Lorentzian function) red shifts by 1.77 cm^{-1} upon strain, indicative of lattice expansion, and in agreement with literature. (E) The A_{1g} (422.39 cm-1 peak ((fitted with Lorentzian function) that defines the out-of-plane vibration is also red-shifted by 1.06 cm^{-1} upon strain, and (F) Strain induced red-shifts in the direct gap transition peak in both mono-and multi-layered WS_2, indicative of band-gap shortening

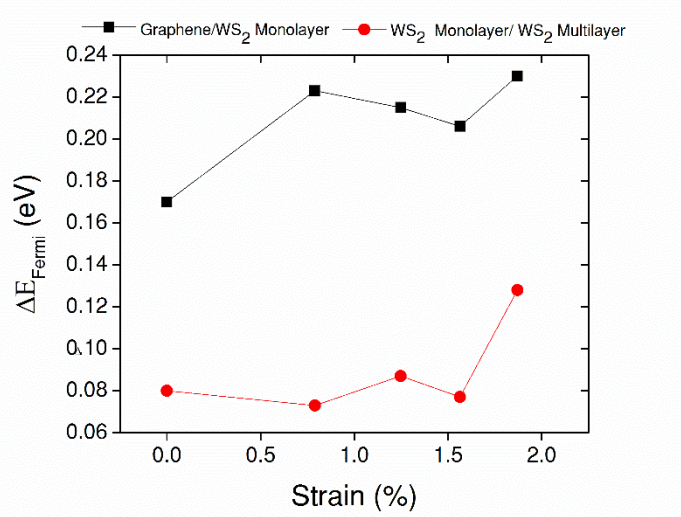

Figure S9. Plot illustrating strain modulated junctions in sample 2. Strain can either increase or decrease the Schottky barrier height and built-in potentials at the Graphene/WS_2 and monolayer WS_2/multi-layer WS_2 interfaces, respectively, due to anisotropic modulation in the work functions.

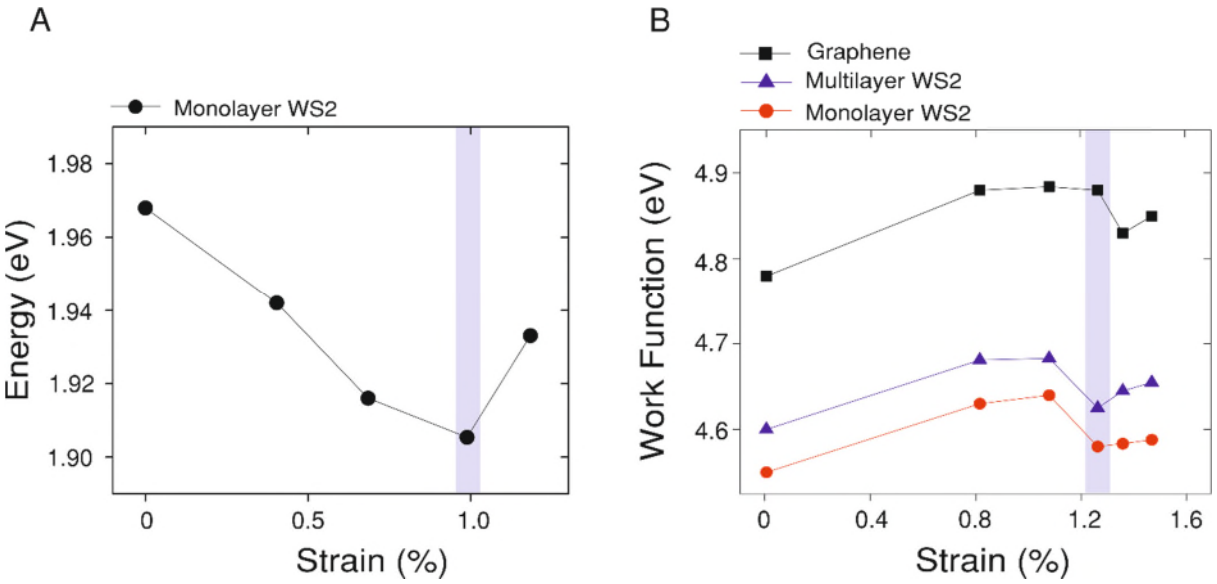

Figure S10 (A and B). (A) Photoluminescence spectroscopy (PL) studies of the Graphene/WS_2 heterostructure as a function of uniaxial tensile strain. The exciton peak position red shifts with increasing strain. This is indicative of band gap shortening. At 1% strain we observe an increase, which we attribute to slippage, and (B) Slippage induced relaxation in Graphene and WS_2 observed in the KPM measurements from another WS_2 domain in sample 1 (note that several WS_2 domains sit on graphene, each of which is expected to strain differently due to different –crystal orientations, -edge geometries and -local substrate roughness). The work function drops at 1.26% strain, and then continues to increase as a function of strain.

References:

[1] Sheng, Y.; Rong, Y.; He, Z.; Fan, Y.; Warner, J.H.; *Nanotechnology* **2015**, *26*, 395601

[2] Feng, Y.; Zhang, K.; Li, H.; Wang, F.; Zhou, B.; Fang, M.; Wang, W.; Wei, J.; Wong, H.S.P. *Nanotechnology* **2017**, *28*, 295705

[3] Lee, S.Y.; Kim, U.J.; Chung, J.; Nam, H.; Jeong, H.Y.; Han, G.H.; Kim, H.; Oh, H.M.;, Lee, H.; Kim, H.; Roh, Y.H.; Kim, J.; Hwang, S.W.; Park, Y.; Lee, Y.H. *ACS Nano* **2016**, *10*, 6100-6107

[4] Pinto, H.; Markevich, A. *Beilstein J. Nanotechnol.* **2014**, *5*, 1842-1848